Journal of Materials Chemistry A

Accepted Manuscript

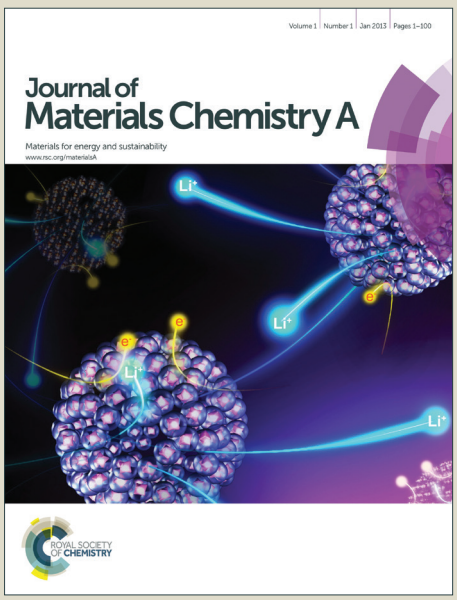

ROYAL SOCIETY OF CHEMISTRY

www.rsc.org/materialsA

A table of contents

Hydrophilic surface modified carbon electrode shows a good electrolyte affinity to give a high volumetric capacitor with the low ion-transfer resistance.

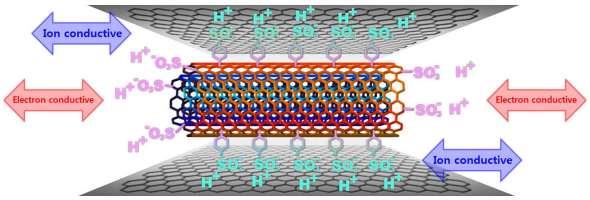

Journal of Materials Chemistry A

RSCPublishing

ARTICLE

Low ion-transfer resistant and high volumetric supercapacitor using hydrophilically surface modified carbon electrodes

Cite this: DOI: 10.1039/x0xx00000x

Heejoun Yoo[a], Misook Min[b], Sora Bak[b], Yeoheung Yoon[a] and Hyoyoung Lee[a,b*]

Received 00th January 2014,
Accepted 00th January 2014

DOI: 10.1039/x0xx00000x

www.rsc.org/

Hydrophilic surface modified carbon electrode shows a good electrolyte affinity with a homogenous dispersibility in water, resulting in the low ion-transfer resistance and the uniform and dense electrode to give a high volumetric capacitor. The hydrophilic carbon electrode exhibits a superior capacitance (58 F cm^{-3}, 99.3 mF cm^{-2}) and is stable up to 5000 cycles.

Introduction

Recent increases in the use of various portable and flexible electronics has generated a growing demand for advanced energy storage devices that are both lightweight, flexible, high efficient and short charging time.[1] Supercapacitors have been received a great deal of attention as next generation energy storage systems due to their outstanding characteristics such as high power density, long cycle life, safety, fast charge-discharge rate, and high efficiency.[2-10] Supercapacitors have a simple charge storage and release mechanism based on an electrostatic interaction between the electrolyte and electrode surface called electrical double layer capacitance (EDLC).[2-6] The simplicity of this mechanism of energy storage allows for the number of advantages.

On the supercapacitors based on EDLCs, the low resistance of electrode material and the high accessibility with electrolyte are the most decisive factor. To achieve high accessibility and penetration of ions from the electrolyte into the electrode, several composite designs have been adopted such as graphene-CNT[7] (carbon nanotube) and graphene-CDC[8] (carbon derived carbon). The CNT and CDCs can effectively exfoliate graphene sheets and prevent restacking, resulting in enhanced electrolyte accessibility.[2,7,8] Another interesting attempt to enhance ion accessibility is using the in-plane or vertical structures, which successfully increase ion accessibility and penetration between two vertically aligned electrodes, resulting in high capacitance and low ion-transfer resistance compared to the common 2D-stacked normal supercapacitors.[9]

On the other hand, additional strong demands for the power sources for portable electronics requires compactness and integration with other electronic components like solid chips type device.[9-13] In addition, miniaturizing power sources into the solid-chip design devices can potentially increase the density of electronic devices with various functions and expand their applications.[9,10] Despite these advances, low energy density remains the biggest challenge and obstacle for the realization of carbon-based supercapacitors.[14] Practically, the volumetric specific capacitance (F cm^{-3}) and areal specific capacitance (F cm^{-2}) of supercapacitors based on carbon materials is much low due to their low density (g cm^{-3}). Likewise, the thickness of electrodes on supercapacitor with common 2D stack structures is strongly restricted with a few micrometres and a much low loading amount due to low ion diffusion and penetration property into the electrode, and thus usually exhibits a much low volumetric specific capacitance (3-50 mF cm^{-2} or less) and restrict realization of supercapacitor.[5, 11, 15] As previous studies, the laser-scribed graphene electrode show 4.04 mF cm^{-2} areal capacitance and less than 0.5 F cm^{-3} volumetric capacitance with H_2SO_4-PVA solid electrolyte.[5] The all-solid-state micro-SC based on graphene and H_3PO_4-PVA show 0.462 mF cm^{-2}.[13] The micro-SC using graphene and CNT composite electrode exhibit 6.1 mF cm^{-2} at 10mV s^{-1}.[23] Actually, there are many studies concerning rGO/CNT composite with superior capacitance performance. Most of them checked capacitance property under solution electrolyte and 3 electro measurement system. Still, the study about solid-state supercapacitor is rare and show too low volumetric capacitance even though using rGO/CNT composite electrode. (see the comparison tables in Table S1 for rGO/CNTs supercapacitors and Table S2 for Solid-state supercapacitors).

In here, we demonstrate a low resistant and high volumetric on-chip type solid-state supercapacitor (SSC) using hydrophilic surface modified multi-walled CNTs (MWCNTs) and reduced graphene oxides (RGOs). The hydrophilic surface modified carbon electrode is expected to show a good electrolyte affinity

and a homogenous dispersibility in water, resulting in the low resistance and the uniform dense electrode to give high volumetric capacity. Especially, for the good accessibility of electrolyte into the carbon-based electrode, we carefully design the surface modified MWCNTs with a hydrophilic sulfonate groups ($R\text{-}SO_3^-$), which allow a hydrophilic surface of the outer carbon nanotube, while keeping high electric conductivity through inner carbon nanotube. Different from previous results, this hydrophilic carbon composite film electrodes exhibit much lower series resistance and simultaneously lower charge-transfer resistance despite its high dense structure (over 0.9 g cm^{-3}).

Experimental

Preparation of diazonium salts

4-Benzenediazoniumsulfonate was synthesized by diazotization of p-sulfonic acid (Aldrich). In a three-necked round flask, 12.99 g (0.075 mol) of p-sulfonic acid was dispersed in 1 M HCl. To the well-stirred suspension in an ice-water bath (3-5 ℃), a 10 % excess of 1 M aqueous solution of $NaNO_2$ (82.5 ml) was added. Solid p-sulfanilic acid was slowly dissolved during of the addition of $NaNO_2$ and a clear solution was obtained after all of the $NaNO_2$ solution was added. The resulting mixture was then stirred for another 45 min at the same temperature. A white precipitate formed and was collected by filtration, washed with cold water, and then dried under vacuum.

Preparation of SCNTs

200 mg of MWCNTs were added to a three-necked round flask with 10 ml of distilled water and 10 ml of ethanol. The mixture was then sonicated for 30 min and cooled to 0-5 ℃ with an ice bath. Next, 10 ml of hypophosphorous acid (H_3PO_2, 50 %, Aldrich) and a prepared 4-Benzenediazoniumsulfonate powder (1.2 g) were added to the MWCNT mixture under stirring. After stirring for 1 h, an additional 10 ml of a H_3PO_2 aqueous solution was added. The mixture was then stirred at 5 ℃ for another 6 h. The resulting product was filtered with a nylon membrane (0.45 ㎛, Whatman) and repeatedly washed with distilled water. Finally, the product powder was dispersed in D.I. water with 0.5 mg ml^{-1} by sonication, and left to stand for 2~3 days. The resulting SC solution without sedimentation was collected and dried at R.T.

Preparation of film-RGO-SCNT and spray-RGO-SCNT electrodes

Graphene oxide (GO) was prepared from natural flake graphite (Bay Carbon, SP-1) by an improved method that was previously described.[20] GO was disperse into distilled water at a concentration of 1 mg ml^{-1} and a SCNT dispersion was also prepared using distilled water with 0.5 mg ml^{-1}. The SCNT solution was then added to the GO solution under stirring. The resulting mixture was sonicated for 1 h, and filtered by vacuum filtration with an anodisc (0.2 ㎛, with support ring, Whatman). After drying in a vacuum oven (60 ℃), the GO-SCNT composite films were reduced by HI vapor reduction with 0.2 ml of HI (57 wt%, Aldrich) and 0.5 ml of acetic acid (99.5 wt%, OCI company Ltd.) in a 300 ml chamber at 40 ℃ for 24 h.[21] For spray-RGO-SCNT electrodes, the dispersed mixture solution of GO and SCNTs was sprayed using a spray-gun with a specific pattern mask on a PET substrate, which was heated to 100 ℃ during the spraying process. After spray coating, the pattern electrode was dried under vacuum at 60 ℃ for 24 h. The dried electrode was then reduced by hydrazine (35 %, 0.3 ml, Aldrich) vapour reduction in a 300 ml chamber at 90 ℃ for 24 h. After reduction, the electrode was repeatedly washed with D.I, and then dried under vacuum at 60 ℃ for 24 h.

Fabrication of supercapacitor cells

To prepare film electrode supercapacitors, as–prepared electrode films were cut into 10 mm x 5 mm square pieces. The two pieces of electrode films were placed on opposite sides of the PET substrate with a 0.2-0.3 mm gap and attached with ketone tape. Pt foil (thickness; 0.1 mm) was used as a current collector, and was also attached using ketone tape covering the electrode films with a width of 0.2 mm. A PVA (10 wt% with H_2O) solution containing 10 wt% of H_2SO_4 was then cast on the electrodes. After drying on a clean bench for 1 day to remove excess H_2O, electrochemical measurements were carried out. Spray pattern electrodes were fabricated by the same procedure using Pt foil and an H_2SO_4/PVA electrolyte.

Characterization

Microstructural characterization was performed using a JEOL JSM-7404F field emission scanning electron microscope operating at 15 kV. XPS measurements were made using a Thermo VG Microtech ESCA 2000 with a monochromatic Al-K X-ray source at 100W. Water contact angle FT-IR spectra were collected using a Thermo Nicolet AVATAR 320 instrument. Contact angles were measured using a SEO Phoenix 300 microscope.

Electrochemical characterization

Cyclic voltammetry of SSCs were measured at various scan rates. Volumetric capacitance derived from CV curves was calculated according to the following equation: $C = 2(\int IdV)/(sv\Delta V)$, where I is the voltammetry current, s is the potential scan rate, V is the potential for one sweep segment, and v is the volume of one electrode. The galvanostatic charge-discharge curves of SSCs were obtained at 2 mA cm^{-2}. The volumetric capacitance derived from galvanostatic discharge curves was calculated based on the following equation: $C = 2(I\Delta t)/(v\Delta V)$, where is I is the discharge current, Δt is the time to full discharge, v is the volume of one electrode, and ΔV is the change in potential during discharge. The effective series resistance (ESR) was estimated using the voltage drop at the beginning of the discharge, V_{drop}, at certain constant current I_{cons}, with formula $R_{ESR} = V_{drop}/(2I_{cons})$ calculated by Energy density (E) and power density (P) were calculated from galvanostatic discharge curves by the equations $E = (1/8)C\Delta V^2$

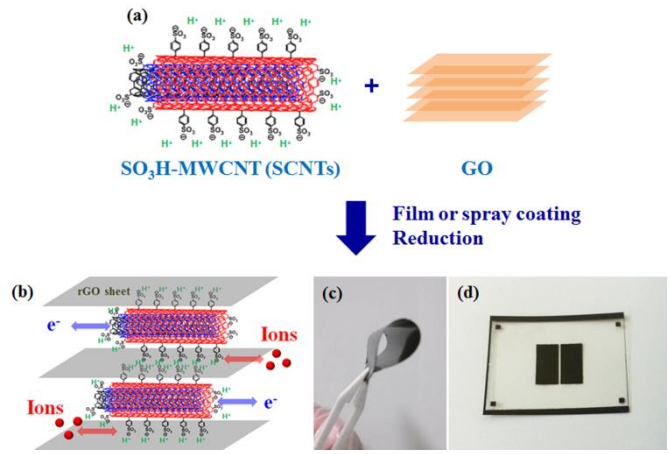

Fig.1 Schematic fabrication process of RGO-SCNT electrodes and images of (a) SCNTs. (b) RGO-SCNT electrodes. Optical images of (c) film-RGO-SCNT electrodes. (d) spray-RGO-SCNT electrode on the PET substrate.

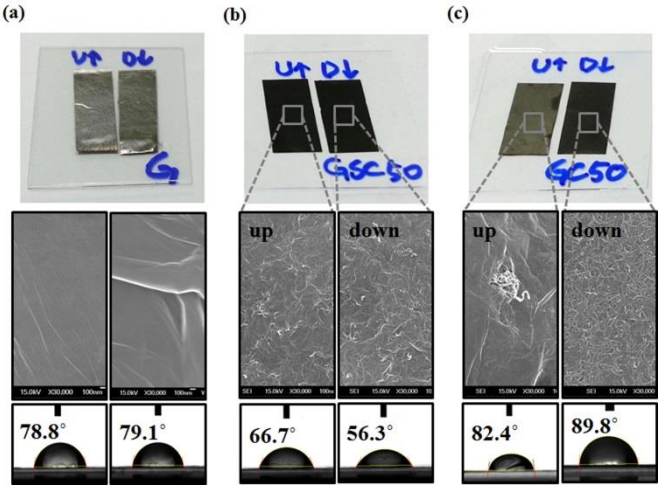

Fig. 2 Optical images, SEM images (up and down side), and water contact angles (up and down side) of (a) RGO electrode films, (b) RGO-SCNT50 electrode films, and (c) RGO-CNT50 electrode films.

and P = E/Δt, where C is the volumetric capacitance, ΔV is the change in potential during discharge, and Δt is the time to full discharge. The electrochemical impedance spectroscopy measures were performed over a frequency range from 10^6 to 10^{-2} Hz using a CHI660D electrochemical workstation. Based on a RC model, the capacitance was also calculated from the frequency response analysis, by C = -1/(2πfZ"), where f is frequency in Hz and Z" is the imaginary part of the impedance, to show the trend of changes in capacitance with frequency.[4]

Result and discussion

As expected, the sulfonate functionalized MWCNTs (SCNTs, Fig. 1a) are well-dispersed in water and freely mixed with graphene oxide (GO) to give a uniform GO-SCNT film, followed by reduction of GO-SCNT to finally give reduced graphene oxide (RGO-SCNT) films (Fig. 1b). Flexible and uniform film electrodes (Fig. 1c) are fabricated by vacuum filtration using an anodisc, and the specific patterned electrodes on the PET substrate (Fig. 1d) are prepared through a simple spray coating process with a patterned mask. The density of RGO-SCNT is approximately 40 vol% smaller than that of the normal RGO-CNT. The resulting high density of the RGO-SCNT film is attributed to the homogeneously mixed SCNTs without aggregation into the graphene sheets, which result in a better packing structure (Fig. S2). For the hydrophilic-surface modified SCNTs, the aryl diazonium salts of sulfanilic acid are prepared as previously described and confirmed by 1H NMR (Fig. S1).[16] Surface functionalization of CNTs with aryl diazonium salts is performed by a chemical diazotization reaction using hypophosphorous acid (H_3PO_2, 50%, Aldrich)[17] and repeatedly washed with large amount of DI water after reaction. The as-prepared SCNTs are then characterized by Fourier transform infrared spectroscopy (FT-IR) and X-ray photoelectron spectroscopy (XPS) and compared with CNTs. FT-IR spectra of SCNTs (Fig. S3b) reveal differential adsorption features such as sharp peaks at 1036 cm^{-1} and a broad peak around 1190 cm^{-1}, which corresponded to the symmetrical and asymmetrical vibrational adsorptions of the SO_3 group, respectively. The peak observed at 1120 cm^{-1} is assigned to the in-plane bending vibration of the benzene ring.[18]

The XPS spectra from SCNTs exhibited peaks at 168.03 eV and 532.12 eV, which originated from SO_3 groups. The S and O contents of SCNTs are 2.8 and 13.8 at%, respectively. Hydrophilic-surface treated SCNTs are completely different from normal CNTs, in that they are freely dispersed in water through the simple sonication (Fig. S3a). The SCNT solution (1 mg ml^{-1} and 0.01 mg ml^{-1} in H_2O) can be uniformly mixed with a GO solution, and homogeneous and flexible RGO-SCNT films are subsequently prepared.

After HI vapor reduction, reference RGO films has a bright grey color and flat surface morphology according to field emission scanning electron microscopy (FE-SEM) images on both the up and down sides of the film (Fig. 2a). An RGO-SCNT50 composite film is prepared by mixing 50 wt% SCNTs and 50 wt% GO, followed by reduction of the mixed films. The RGO-SCNT50 film show the almost same black color on the both sides of the film and exhibited uniformly dispersed CNTs with a bundled microstructure and less aggregation into the side and black on the down side of films (Fig. 2b). The black colored down-side morphology of RGO-CNT50 films is attributed to aggregation of CNTs bundles while the grey colored up side is attributed to exposure of RGO sheets, indicating that the CNT bundles are sparsely mixed with RGO sheets (Fig. 2c). On the other hand, according to the water contact angle, RGO films exhibit hydrophobic surface properties typical of chemically reduced graphene films.[21] As expected, RGO-SCNT50 films has high hydrophilic surface (water contact angle; 66.7° and 56.3° on the up and down sides of films, respectively) due to presence of SO_3H functional groups of SCNTs, and is significantly different from that of the RGO and RGO-CNT50 films. On the other hand, the down side of RGO-SCNT50 in comparison with the up side is more hydrophilic due to higher sedimentation of SCNT at down-side

Journal of Materials Chemistry A

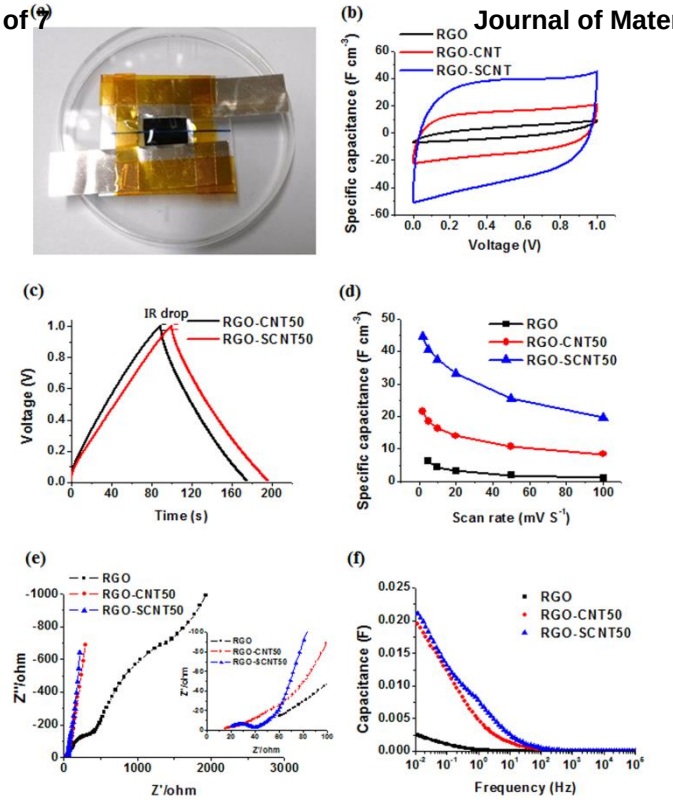

Fig. 3 (a) Photo image of proto type solid-state supercapacitor cell, (b) CV curves of RGO, RGO-CNT50 and RGO-SCNT50 at scan rate of 20 mV sec^{-1}, (c) galvano charge/discharge at constant 2 mA cm^{-2}, (d) Volumetric capacitance with different scan rate from 2 to 100 mV sec^{-1}, (e) Nyquist impedance plots, (f) Frequency response versus capacitance.

during vacuum filtration process. RGO-CNT50 films exhibit more hydrophobic surface (82.4° and 89.8° on the up and down sides of the film, respectively), which is due to the strong hydrophobic properties of CNTs. The bottom-side of RGO-CNT50 in comparison with up-side is more hydrophobic due to more existence of CNTs at the bottom side.

We investigate the capacitance performance through the in-planar symmetrical two-electrode system. Prototype solid-state supercapacitor cells (Fig. 3a) are fabricated with as-prepared RGO-SCNT50 film electrodes (5 mm x 10 mm) and Pt foil (5 mm x 30 mm x 0.1 mm) as the current collector and then attach on PET substrate. The as-prepared solid-state supercapacitors are evaluated by cyclic voltammetry (CV), galvanostatic charge-discharge, and Nyquist impedance plots. Fig. 3b shows the CV curves of RGO, RGO-CNT50, and RGO-SCNT50 at 20 mV sec^{-1}. RGO exhibits a narrow curve shape, whereas RGO-CNT50 and RGO-SCNT50 exhibit a rectangular curve shape. RGO-SCNT50 has the largest specific capacitance (33.2 F cm^{-3}), while RGO-CNT50 and RGO exhibit capacitance values of 14 F cm^{-3} and 3.3 F cm^{-3} at the same scan rate, respectively. The specific capacitance and ESR calculated from galvanostatic charge-discharge curves (Fig. 3c and Fig. S4, detail voltage drop) for RGO-SCNT50 are 29.4 F cm^{-3} and 29.7 Ω, while those of RGO-CNT50 are 12.9 F cm^{-3} and 43.3 Ω, respectively. The RGO-SCNT50 exhibits superior capacitance property and lower ESR than those of RGO-CNT50 and RGO. Fig. 3d shows the specific capacitance versus scan rate from 2 to 100 mV sec^{-1}. The specific capacitance of RGO-SCNT50 is 44.5 F cm^{-3} at 2 mV sec^{-1} and decay to 20 F cm^{-3} as the scan rate increased to 100 mV sec^{-1}. Similarly, the capacitances of RGO-CNT50 and RGO decay from 21.4 F cm^{-3} to 8.4 F cm^{-3} and from 8.2 F cm^{-3} to 1.2 F cm^{-3}, respectively (Fig. 3d). Frequency response analysis (FRA) over a frequency range from 10^{6} to 10^{-2} Hz yielded the Nyquist plots for RGO-SCNT50, RGO-CNT50 and RGO are shown in Fig. 3e. Plots of RGO-SCNT50 and RGO-CNT50 featured vertical curves, which are different from RGO, indicating nearly ideal capacitive behaviour. The typical Nyquist plot of supercapacitor can be classified into the three regions following the frequency range. At high frequency, the intersection point on the real axis (Z') represents the ohmic resistance of the electrolyte and the internal resistance of the electrode, which is described as series resistance (R_S). The semi-circular plot in the high to middle frequency range corresponds to the parallel connection of the ion transfer resistance (R_{IT}) and the EDLC. The transition from the semicircle to the long tail is attributed to the ion diffusion to the inside electrode.[22] Based on the magnified curve in the high-frequency range (Fig. 3e, inset), the R_S and R_{IT} are 20.2 Ω and 19.2 Ω for RGO-SCNT50, 15.5 Ω and 53 Ω for RGO-CNT50, and 60 Ω and over 380Ω for RGO, respectively. The R_S of RGO-CNT50 and RGO-SCNT50 are lower than that of RGO, suggesting that the enhanced electric conductivity of electrode is due to the presence of CNTs and SCNTs. As expected, the R_S of RGO-SCNT50 is slightly higher than that of RGO-CNT50, which can be explained by the aromatic SP3 defects of SCNTs resulting from outer carbon surface functionalization. Furthermore, the R_{IT} of RGO-SCNT50 and RGO-CNT50 are much lower than that of RGO and the slope of linear plot after semicircle transition are steeper, suggesting better accessibility and low ion-transfer resistance of the electrolyte. In contrast, RGO exhibit a non-ideal capacitive curve and high R_{IT}, suggesting very poor accessibility of the polymer electrolyte and high resistance. Our results indicate that the CNTs are able to function as spacers between RGO sheets, thereby preventing strong restacking of RGO and enhancing electrolyte accessibility. Furthermore, the R_{IT} of RGO-SCNT50 is lower and its curve is steeper than that of RGO-CNT50, since SCNTs have hydrophilic SO_3H functional groups on their outer layer that provides easy access of protons from the electrolyte. Simultaneously, the inner layers of SCNTs maintained high electric conductivity, and thus R_S is also effectively decreased. The capacitance from FRA data versus frequency based on a series RC model is shown in Fig. 3f. The capacitance of RGO-SCNT50 is the highest among all of the films tested at all frequency ranges, while RGO exhibit a very small capacitance even at a low frequency range. These results confirm that the superior electrochemical performance of RGO-SCNT50 composite electrodes is due to the enhanced electric conductivity and high accessibility of the electrolyte.

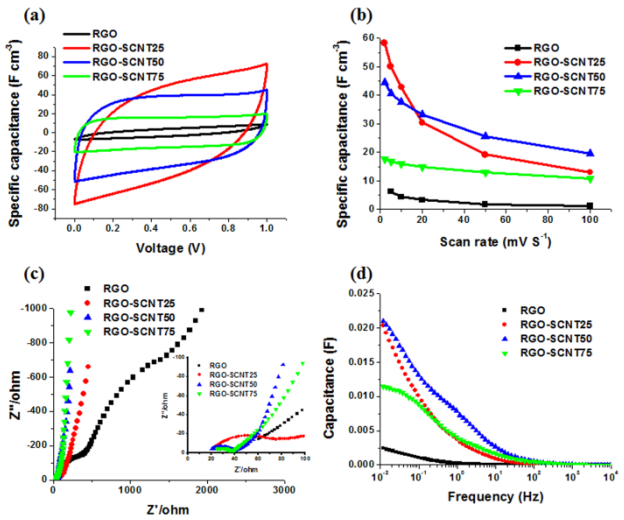

Fig. 4 The supercapacitor performance of the RGO-SCNT electrodes with different contents of SCNTs from 25 to 75 wt%; (a) CV curves at scan rate of 20 mV sec^{-1}, (b) Volumetric capacitance with different scan rates from 2 to 100 mV sec^{-1}, (c) Nyquist impedance plots, (d) Frequency response versus capacitance.

To further evaluate RGO-SCNT electrodes as solid-state supercapacitors, we test RGO-SCNT electrodes with different ratios of SCNT. As the ratio of SCNT increased, CV curves (Fig. 4a) became more rectangular. The CV curves of RGO-SCNT25 exhibit a moderate current increase and decreased shape, while RGO-SCNT75 exhibits a more rectangular curve shape. However, the CV curve area of RGO-SCNT75 is smaller than those of both RGO-SCNT25 and RGO-SCNT50, which is attributed to the active surface area of RGO-SCNT75 decreasing as the amount of CNTs increased. Specific capacitance versus scan rate is presented in Fig. 4b. RGO-SCNT25 exhibit the highest capacitance value at a low scan rate, but its capacitance sharply decreased from 58.4 F cm^{-3} to 13 F cm^{-3} as the scan rate increased from 2 to 100 mV sec^{-1}, ultimately decreasing with 77.7%. Likewise, the capacitance of RGO-SCNT75 decreased from 17.2 F cm^{-3} to 12.9 F cm^{-3}, eventually decreasing with 25%. RGO-SCNT75 has a lower capacitance than the other RGO-SCNTs; however, it exhibited a superior rate-capacitance.

RGO-SCNT50 exhibits a rather modest capacitance decay curve compared with RGO-SCNT25, exhibiting the highest capacitance at scan rates greater than 20 mV sec^{-1}. Fig. 4c shows Nyquist plots of RGO, RGO-SCNT25, RGO-SCNT50 and RGO-SCNT75. All RGO-SCNT samples exhibit vertical, steeper curves. Based on magnified curves in the high-frequency range (Fig. 4c and inset), RGO-SCNT25 is determined to have a relatively larger semi-circle and high R_{CT} of over 60 Ω, while RGO-SCNT75 exhibit a smaller semi-circle and R_{CT} of 12.3 Ω. In addition, the plot after semi-circle transition is steeper as amount of SCNT, which is suggesting better accessibility to the electrolyte. Interestingly, the R_S of RGO-SCNT75 (24.6 Ω) is higher than that of RGO-SCNT25 (20.8 Ω) and RGO-SCNT50 (20.2 Ω). This result is possibly due to a low packing density between RGO sheets and CNT bundles. The electric conductivity of electrodes is strongly affected by packing density.[19] Indeed, the bulk-density of RGO-SCNT75 (0.64 g cm^{-3}) is much lower than that of RGO-SCNT25 (0.94 g cm^{-3}) and RGO-SCNT50 (0.9 g cm^{-3}). With respect to hydrophilicity, the water contact angles (WCAs) of RGO-SCNT film electrodes (Fig. S5) are slightly different between the up and down sides. Specifically, the down side of RGO-SCNT films is slightly more hydrophilic (with lower WCA) than that of the up side, which is possibly due to accumulation of vacuum force during production of the film electrode by the vacuum filter method. In addition, WCA decreased as the ratio of SCNTs increased, which resulted in increased hydrophilicity. These results are consistent with our observation of a low ion-transfer resistance as the ratio of SCNTs increased. Fig. 4d shows the capacitances from FRA data versus frequency of the RGO-SCNT sample series; RGO-SCNT50 exhibit the highest capacitance among all of the other samples at all frequency ranges.

We evaluate RGO-SCNT50 for electrochemical stability by CV at 100 mV sec^{-1}. RGO-SCNT50 maintains a specific capacitance of approximately 93 % of the initial value after 5000 cycles (Fig. S7), indicating good electrochemical stability. Table S1 summarizes the specifications of electrodes such as volumetric specific capacitance value, water contact angles, and resistance properties obtained from Nyquist plots.

To demonstrate on-chip solid-state supercapacitors with specific patterns, we fabricate RGO-SCNT50 capacitor cells on a PET substrate using a spray coating method with patterned mask (Fig. 1d and movie clip S1). FE-SEM images of spray-RGO-SCNT50 are shown in Fig. 5b and compared with RGO-SCNT50 up side (Fig. S6a). Spray-RGO-SCNT50 has a coarser surface morphology. In addition, the spray-RGO-SCNT50 has a lower density (0.7 g cm^{-3}) than that of the RGO-SCNT50 film (0.9 g cm^{-3}). The WCA of the spray-RGO-SCNT50 was 64°, which is similar to that of the spray-RGO-SCNT50. The capacitance performance of the spray-RGO-SCNT50 evaluated by CV curves at different scan rates and is similar to that RGO-SCNT50 film, suggesting that there is no difference in electrochemical properties for spray coating and vacuum filter process (Fig. S6c and S6d).

Conclusions

In summary, we demonstrate a low ion-transfer resistant and high volumetric on-chip solid-state supercapacitors consisting of hydrophilic MWCNTs and graphene flakes, and an H_2SO_4/PVA electrolyte. The specially designed hydrophilic MWCNTs are prepared by chemical attachment on the outer surface of MWCNTs by reduction of para-sulfonic phenyl diazonium salt with hypophosphorous acid, and are freely dispersed in water and can be mixed well with GO solution, ultimately leading to a uniform RGO-SCNT film through reduction of a GO-RGO film. Hydrophilic treated SCNTs on the outer surface of MWCNTs exhibit a high electric conductivity throughout the inner layers of MWCNTs. Therefore, RGO-SCNT composite electrodes exhibit a low wetting angle as well as low ion-transfer resistance. In addition, the homogenously dispersed RGO-SCNT solution in water

gave a high volumetric capacitance with high packing density and it is easily applied for fabrication of specific patterned electrodes by a spray coating technique, allowing integration onto one flexible chip with specific patterns. RGO-SCNT films exhibit the highest capacity and rate-capacitance properties and stable, maintaining a capacitance of 93 % of the initial value after 5,000 cycles. In addition, the solid-state spray-RGO-SCNT electrodes can be connected in series or in parallel to improve overall output potential and/or current. In addition, they may also be integrated onto various substrates for energy storage devices, including portable, stretchable, and wearable electronic devices.

Acknowledgements

This work was supported by the National Research Foundation of Korea (NRF) grant funded by the Korea government (MSIP) (Grant No. 2006-0050684 and Grant No. B551179-13-01-01).

Notes and references

[a] NCRI, Center for Smart Molecular Memory, Department of Energy Science, Sungkyunkwan University, 2066 Seoburo, Jangan-gu, Suwon, Gyeonggi-do 440-746, Republic of Korea.
[b] NCRI, Center for Smart Molecular Memory, Department of Chemistry, Sungkyunkwan University, 2066 Seoburo, Jangan-gu, Suwon, Gyeonggi-do 440-746, Republic of Korea.

† Electronic Supplementary Information (ESI) available: Experimental section, supporting figures and data tables, Movie clips See DOI: 10.1039/c000000x/

1 D. Pech, M. Brunet, H. Durou, P. H. Huang, V. Mochalin, Y. Gogotsi, P. L. Taberna, P. Simon, Nat. Nanotechnol., 2010, **5,** 651; Z. Niu, H. Dong, B. Zhu, J. Li, H. H. Hng, W. Zhou, X. Chen, S. Xie, Adv. Mater., 2013, **25**, 1058; H. Yoo, Y. Kim, J. Lee, H. Lee, Y. Yoon, G. Kim, H. Lee, Chem. Eur. J., 2012, **18**, 4923.
2 H. M. Jeong, J. W. Lee, W. H. Shin, Y. J. Choi, H. J. Shin, J. K. Kang, J. W. Choi, Nano Lett., 2011, **11**, 2472; Y. Zhai, Y. Dou, D. Zhao, P. F. Fulvio, R. T. Mayes, S. Dai, Adv. Mater., 2011, **23**, 4828.
3 P. Simon, Y. Gogotsi, Nat. Mater., 2008, **7**, 845; M. D. Stoller, S. Park, Y. Zhu, J. An, R. S. Ruoff, Nano lett., 2008, **8**, 3498.
4 Y. Zhu, S. Murali, M. D. Stoller, K. J. Ganesh, W Cai, P. J. Ferreira, A. Pirkle, R. M. Wallace, K. A. Cychosz, M. Thommaes, D. Su, E. A. Stach, R. S. Ruoff, Science, 2011, **332**, 1537.
5 M. F. El-Kady, V. Strong, S. Dubin, R. B. Kaner, Science, 2012, **335**, 1326.
6 Y. Xu, G Shi, J. Mater. Chem., 2011, **21**, 3311; Z-S. Wu, A. Winter, L. Chen, Y. Sun, A. Turchanin, X. Feng, K. Mullen, Adv. Mater., 2012, **24**, 5130; Y. Li, Z. Li, P. K. Shen, Adv. Mater., 2013, **25**, 2474.
7 A. L. M. Reddy, S. R. Gowda, M. M. Shaijumon, P. M. Ajayan, Adv. Mater., 2012, **24**, 5045; Z. Fan, J. Yan, L. Zhi, Q. Zhang, T. Wei, J. Geng, M. Zhang, W. Qian, F. Wei, Adv. Mater., 2010, **22**, 3723; N. Jha, P. Ramesh, E. Bekyarova, M. E. Itkis, R. C. Haddon, Adv. Energy Mater., 2012, **2**, 438.
8 M. Heon, S. Lofl, J. Applegate, R. Nolte, E. Cortes, J. D. Hettinger, P.-L. Taberna, P. Simon, P. Huang, M. Brunet, Y. Gogotsi, Energy Environ. Sci., 2011, **4**, 135; Z. Lei, Z. Liu, H. Wang, X. Sun, L. Lu, X. S. Zhao, J. Mater. Chem. A, 2013, **1**, 2313.
9 J. J. Yoo, K. Balakrishnan, J. Huang, V. Meunier, B. G. Sumpter, A. Srivastava, M. Conway, A. L. M. Reddy, J. Yu, R. Vajtai, P. M. Ajayan, Nano Lett., 2011, **11**, 1423.
10 J. Chmiola , C. Largeot , P. L. Taberna , P. Simon , Y. Gogotsi , Science, 2010, **328** , 480.
11 M. Kaempgen, C. K. Chan, J. Ma, Y. Cui, G. Gruner, Nano Lett., 2009, **9**, 1873.
12 M. Beidaghi, C. Wang, Adv. Funct. Mater., 2012, **22**, 4501.
13 Z. Niu, L. Zhang, L, Liu, B. Zhu, H. Dong, X. Chen, Adv. Mater. 2013, **25**, 4035.
14 Y. Xu, Z. Lin, X. Huang, Y. Liu, Y. Huang, X. Duan, ACS Nano, 2013, **7**, 4042.
15 M. D. Stoller , R. S. Ruoff, Energy Environ. Sci., 2010, **3**, 1294; Z. Weng, Y. Su, D.-W. Wang, F. Li, J. Du, H.-M. Cheng, Adv. Energy Mater., 2011, **1**, 917.
16 Q. Li, L. Dong, F. Sun, J. Huang, H. Xie, C. Xiong, Chem. Eur. J., 2012, **18**, 7055.
17 X. Wang, R. Liu, M. M. Waje, Z. Chen, Y. Yan, K. N. Bozhilov, P. Feng, Chem. Mater., 2007, **19**, 2395; M. Pandurangappa, N. S. Lawrence, R. G. Compton, Analyst, 2002, **127**, 1568.
18 C. Y. Du, T. S. Zhao, Z. X. Liang, Journal of Power Sources, 2008, **176**, 9; J. C. Yang, M. J. Jablonsky, J. W. Mays, Polymer, 2002, **43**, 5125.
19 I. K. Moon, J. I. Kim, H. Lee, W. C. Kim, H. Lee, Scientific Reports 2013, **3**, 1112.
20 D. C. Marcano, D. V. Kosynkin, J. M. Berlin, A. Sinitskii, Z. Sun, A. Slesarev, L. B. Alemany, W. Lu, J. M. Tour, ACS Nano, 2010, **4**, 4806.
21 I. K. Moon, J. Lee, R. S. Ruoff, H. Lee, Nat. Commun., 2010, **1**, 73.
22 B. G. Choi, J. Hong, W. H. Hong, P. T. Hammond, H. Park, ACS Nano, 2011, 5, 7205; C. Masarapu, H. F. Zeng, K. H. Hung, B. Wei, ACS Nano, 2009, **3**, 2199.
23 M. Beidaghi, C. Wang, Adv. Funct. Mater., 2012, 22, 4501.

